not inconsistent with the expected presence of additional Cu atoms in a compact cluster structure.

Edge and Near-Edge Structure (XANES). The energies and intensities of fine-structure features in the edge and near-edge region of the absorption spectrum (0-50 eV above the threshold energy) are also useful probes of the electronic and geometric environment of the absorbing Cu atom. The expanded edge spectra of Cu thionein, the aforementioned Cu_4S_6 cluster model, and a linear two-coordinate Cu complex are shown in Figure 4. Each of the spectra reveal a feature on the rising portion of the edge at 8984 eV. For the two-coordinate complex, this feature is very intense and much better resolved. Polarized edge studies on a series of Cu(I) and Cu(II) model compounds revealed that this type of feature of the rising portion of the edge (found at 8983-8984 eV for Cu(I) and 8986-8987 eV for Cu(II)) is most readily assigned to a 1s → 4p transition.[21] It is most intense in highly anisotropic ligand fields such as linear and square-planar geometries and is strongly polarized along the direction of minimum ligand interaction. Linear Cu(I) models typified by the complex shown in Figure 4 exhibit 1s → 4p transitions in the 8983-8987-eV region that appear as resolvable edge features more intense than the observed shoulder in the edge of Cu-MT or the three-coordinate Cu_4S_6 model complex.[22] This observation is consistent with three- or four-coordinate geometry around Cu in Cu-MT and a more symmetric Cu environment than that indicated by the previously proposed two-coordinate linear-chain structure. Comparison of the Cu-MT and Cu_4S_6 model edge data reveals similar edge features between the two spectra and provides further evidence for a Cu cluster moiety in Cu-MT. A more quantitative treatment of these effects in Cu(I) and Cu(II) edges for inorganic complexes and proteins will be soon forthcoming.[22]

When they are taken together, these X-ray absorption edge and EXAFS results indicate that the Cu atoms are contained in a compact polynuclear cluster with sulfur (thiolate cysteine) ligation. From EXAFS analysis on solutions, it is not possible to determine geometry, and thus, a detailed structure cannot be proposed. It is worthwhile to note that as the Cu:S ratio approaches 1 in such a compact structure, there will, of necessity, be nonbonded S ligands in closer proximity to Cu atoms if a coordination number of 3-4 is maintained. The alternative for approaching a coordination number of 2 is a more linear, extended structure, the presence of which is shown to be unlikely on the basis of, in particular, the edge results and the EXAFS results described above. Thus, in a compact cluster, the nonbonded contacts could account for the second shell of S atoms possibly present in Cu-MT.

Acknowledgment. This work was supported by NSF Grant CHE-8512129 and Swiss National Foundation Grant 3.285-0.82. T.A.S. was the recipient of an NSF predoctoral fellowship award. The measurements were carried out at the Stanford Synchrotron Radiation Laboratory, which is supported by the U.S. Department of Energy, Office of Basic Energy Sciences, and the National Institutes of Health Biotechnology Resource Program, Division of Research Resources. We thank Dr. D. Coucouvanis for the generous gift of a sample of the Cu_4S_6 complex.[12]

Registry No. Cu, 7440-50-8; S, 7704-34-9.

(21) Smith, T. A.; Penner-Hahn, J. E.; Hodgson, K. O.; Berding, M. A.; Doniach, S. *Springer Proc. Phys.* **1984**,*2*, 58-60.
(22) Kau, L.-S.; Spira-Solomon, D. J.; Penner-Hahn, J. E.; Hodgson, K. O.; Solomon, E. I. submitted for publication in *J. Am. Chem. Soc.*
(23) The periodic group notation in parentheses is in accord with recent actions by IUPAC and ACS nomenclature committees. A and B notation is eliminated because of wide confusion. Groups IA and IIA become groups 1 and 2. The d-transition elements comprise groups 3 through 12, and the p-block elements comprise groups 13 through 18. (Note that the former Roman number designation is preserved in the last digit of the new numbering: e.g., III → 3 and 13.)

Contribution from the Department of Chemistry, Indian Institute of Technology, Madras 600 036, India

Single-Crystal Optical Spectral Studies of Tetrabutylammonium Bis(maleonitriledithiolato)nickelate(II)

G. V. R. Chandramouli and P. T. Manoharan*

Received January 14, 1986

A detailed optical spectral study of $[(n\text{-}Bu)_4N]_2[Ni(mnt)_2]$ carried out in solution and single-crystal media is reported. Polarized optical spectral measurements at 298 K and temperature-dependent spectral measurements with unpolarized light in the range 18-298 K have been carried out. Using the 12 transitions observed in single crystals, we could deconvolute the solution spectrum of this complex to locate all of them. The polarization and allowedness of all the bands have been determined. Vibronic progressions have been resolved on some of the bands at 50 K, where maximum resolution occurred. An unusual temperature dependence of spectral intensities has been observed above and below 50 K and is attributed to changes in the lattice. All the d → d transitions have been identified unlike in the earlier works and the assignments based on the energy level scheme proposed in this work are compared with those of earlier reports. Energy level schemes proposed earlier by WHMO, simple MO, and discrete variational Xα calculations and EPR results have been comprehensively compared with the present spectral data of crystals.

Introduction

During the 1960s there had been a great deal of progress on the synthesis, electronic structures, and reaction mechanisms of square-planar metal complexes involving dithiolenes.[1-16] In the systems RC(=S)C(=S)R the tendency of the sulfur atoms to form covalent bonds with metals is uniquely combined with a high electron affinity of the ligand, leading to metal complexes char-

(1) Schrauzer, G. N.; Mayweg, V. P. *J. Am. Chem. Soc.* **1965**, *87*, 1483.
(2) Schrauzer, G. N.; Mayweg, V. P. *J. Am. Chem. Soc.* **1962**, *84*, 3221.
(3) Schrauzer, G. N.; Mayweg, V. P. *Z. Naturforsch. Anorg. Chem., Org. Chem., Biochem., Biophys., Biol.* **1964**, *19B*, 192. Schrauzer, G. N.; Finck, H. W.; Mayweg, V. P. *Ibid.* **1964**, *19B*, 1080.
(4) Schrauzer, G. N.; Finck, H. W. *Angew. Chem.* **1964**, *76*, 143; *Angew. Chem., Int. Ed. Engl.* **1964**, *3*, 133.
(5) Schrauzer, G. N.; Mayweg, V. P.; Finck, H. W.; Muller-Westerhoff, W.; Heinrich, W. *Angew. Chem.* **1964**, *76*, 345; *Angew. Chem., Int. Ed. Engl.* **1964**, *3*, 381. *Angew. Chem.* **1964**, *76*, 715. *Angew. Chem., Int. Ed. Engl.* **1964**, *3*, 639.
(6) McCleverty, J. A. *Prog. Inorg. Chem.* **1968**, *10*, 49.
(7) Gray, H. B.; Billig, E. *J. Am. Chem. Soc.* **1963**, *85*, 2019.
(8) Billig, E.; Schupack, S. I.; Waters, J. H.; Williams, R.; Gray, H. B. *J. Am. Chem. Soc.* **1964**, *86*, 926.
(9) Davison, A.; Edelstein, N.; Holm, R. H.; Maki, A. H. *Inorg. Chem.* **1963**, *2*, 1227.
(10) Billig, E.; Williams, R.; Bernal, I.; Waters, J. H.; Gray, H. B. *Inorg. Chem.* **1964**, *3*, 663.
(11) Eisenberg, R.; Ibers, J. A.; Clark, R. J. H.; Gray, H. B. *J. Am. Chem. Soc.* **1964**, *86*, 113.
(12) Shupack, S. I.; Billig, E.; Clark, R. J. H.; Williams, R.; Gray, H. B. *J. Am. Chem. Soc.* **1964**, *86*, 4594.
(13) Latham, A. R.; Hascall, V. C.; Gray, H. B. *Inorg. Chem.* **1965**, *4*, 788.
(14) Schrauzer, G. N.; Mayweg, V. P. *J. Am. Chem. Soc.* **1965**, *87*, 3585.
(15) Maki, A. H.; Edelstein, N.; Davison, A.; Holm, R. H. *J. Am. Chem. Soc.* **1964**, *86*, 4580.
(16) Schmitt, R. D.; Maki, A. H. *J. Am. Chem. Soc.* **1968**, *90*, 2288.

0020-1669/86/1325-4680$01.50/0

acterized by many unusual and unprecedented chemical and physical properties. These dithiolene complexes have extremely interesting magnetic, electrical, and optical properties. They also, in general, possess an overall planar geometry irrespective of the metal or its oxidation state. These metal complexes undergo facile reversible electron-transfer reactions, have highly delocalized electronic structure, and are known for their ability to form electron donor–electron acceptor compounds with organic donor molecules to give a D^+A^- salt where D^+ and/or A^- are paramagnetic.[17-27] The formation of such donor–acceptor complexes containing $[Ni(mnt)_2]^{n-}$ ions, where mnt refers to maleonitrile-1,2-dithiolene, and their ability to form columnar crystallographic packing are related to their gross planar character and electronic structure comparable to those of the tetracyanoquinodimethane anion. These compounds also exhibit interesting electron-transfer photochemistry. A recent paper[28] presents the photoelectrochemical studies of a series of $M(mnt)_2^{n-}$ complexes where M = Ni, Pd, Pt, Cu and n = 0–3.

One of the most interesting aspects of the nickel dithiolene complexes is their rich optical spectra. Though there have been many sincere attampts to decipher their electronic structures and then to identify their ground and excited states, there has been some basic discord in the various energy levels proposed.[12-16,29] The ground and excited states have been predicted mainly on the basis of EPR results,[15,16] Wolfsberg–Helmholz molecular orbital calculations,[12] simple molecular orbital calculations,[14] and Xα calculations.[29] There have been differences in the prediction of ground and excited states, since their interpretations were based mainly on the solution spectra. It is well-known that the assignments based on the solution spectra would only be tentative, since the spectra do not give any information regarding their intensity-drawing mechanisms as well as their allowed or forbidden nature. In this work we shall attempt to coordinate all the schemes and give the assignments of various electronic transitions on the basis of crystal spectra measured with polarized light and at different temperatures. Since the energy level ordering in $[Ni(mnt)_2]^-$ and $[Ni(mnt)_2]^{2-}$ is expected to be more or less similar, we have carried out a detailed investigation on the electronic spectral properties of the diamagnetic complex tetrabutylammonium bis(maleonitriledithiolato)nickelate(II) ($[(n\text{-}Bu)_4N]_2[Ni(mnt)_2]$).

Experimental Section

(i) Preparation. The compound $[(n\text{-}Bu)_4N]_2[Ni(mnt)_2]$ was prepared by methods described in the literature.[9,10] Thin red crystals of this complex were grown by slow evaporation of its acetone solution at about 15 °C. The crystals grow as flat prismatic plates, which are suitable for studying the absorption in the highly absorbing regions.

(ii) Spectral Measurements. The morphology given in Figure 1a was determined by the use of known unit cell dimensions[30] and the orientation matrix of the crystal, which was determined with an Enraf-Nonius four-circle automatic X-ray diffractometer. All the absorption spectral measurements were made with either a microspectrophotometer developed in our laboratory or a Varian Cary 2390 spectrophotometer. Measurements were made by keeping the electric vector parallel and perpendicular to the crystallographic c axis and shining light on the most prominent flat face (100) of the crystal. The extinctions were observed by a polarizing microscope in the directions selected for polarizations. The light from the monochromator was polarized with an Oriel Glan prism. A crystal of roughly 4 mm^2 cross section was mounted on a perforated copper foil. This was used directly in the optical path of the spectrometers for room-temperature measurements while the same was mounted on a Cryodyne cryocooler for temperature-dependence measurements. However, polarization measurements were made only at room temperature, while the spectral measurements with unpolarized radiation were made at different temperatures. For polarization purposes the crystal was kept stationary, with changes only in the direction of the electric vector of the light. Since the intensities of infrared bands are weak, a crystal of nearly 1.0-mm thickness was used for measurements in that region.

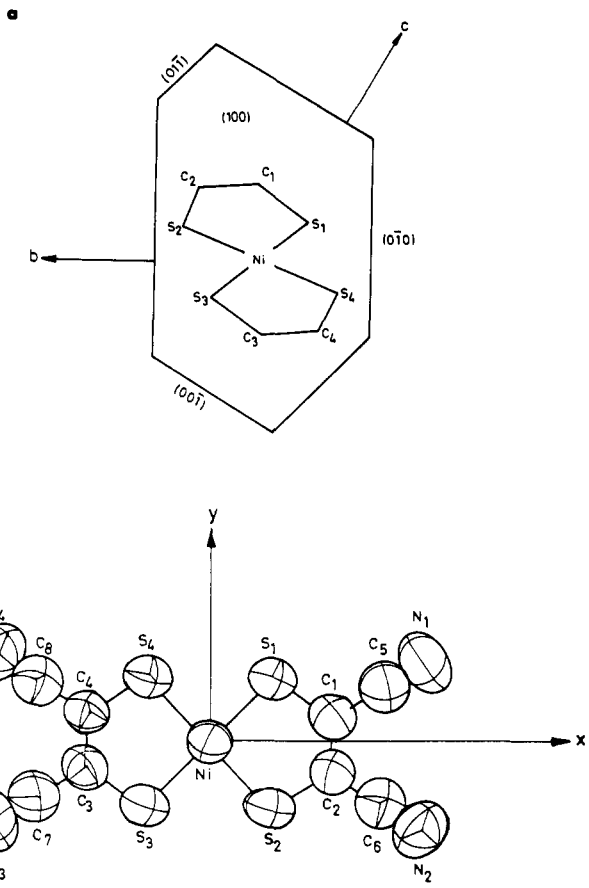

Figure 1. (a) Morphology of $[(n\text{-}Bu)_4N]_2[Ni(mnt)_2]$ and projection of the $Ni(mnt)_2^{2-}$ molecular plane on the (100) plane. (b) Molecular geometry of $Ni(mnt)_2^{2-}$ along with the coordinate system.

Structure of $[(n\text{-}Bu)_4N]_2[Ni(mnt)_2]$

This complex belongs to the space group $P\bar{1}$. The unit cell dimensions are as follows: a = 12.360 Å; b = 11.138 Å; c = 9.833 Å; α = 118.43°; β = 92.05°; γ = 91.91°; Z = 1.[30] The molecular geometry of $[Ni(mnt)_2]^{2-}$ anion is shown in Figure 1b. The planar diamagnetic $[Ni(mnt)_2]^{2-}$ anion has a center of symmetry at the nickel atom, the two cations being related to each other by a center of symmetry. The shortest distance between the adjacent nickel atoms is 9.83 Å, incidating almost no overlap between the nearby complex ions. The Ni–S bond length is 2.176 Å, and the S–Ni–S bond angle within a five-membered ring is 92°. The crystallographic c axis makes an angle of about 38° to the z axis of the molecule, while the line perpendicular to the c axis in the bc plane is almost perpendicular (82°) to the molecular z axis.

Results

The room-temperature solution spectrum of $[(n\text{-}Bu)_4N]_2[Ni(mnt)_2]$ is shown as an energy plot in Figure 2. The spectrum is quite identical with that reported by Shupack et al.[12] except for the presence of two shoulders at 13 750 and 22 110 cm^{-1}. This

(17) Schmitt, R. D.; Wing, R. M.; Maki, A. H. *J. Am. Chem. Soc.* **1969**, *91*, 4394.
(18) Wing, R. M.; Schlupp, R. L. *Inorg. Chem.* **1970**, *9*, 471.
(19) Geiger, W. E., Jr.; Maki, A. H. *J. Phys. Chem.* **1971**, *75*, 2387.
(20) Hove, M. J.; Hoffman, B. M.; Ibers, J. A. *J. Chem. Phys.* **1972**, *56*, 3490.
(21) Wudl, F.; Ho, C. H.; Nagel, A. *J. Chem. Soc., Chem. Commun.* **1973**, 923.
(22) Alcacer, L.; Maki, A. H. *J. Phys. Chem.* **1974**, *78*, 215.
(23) Jacobs, I. S.; Bray, J. W.; Hard, H. R., Jr.; Interrante, L. V.; Kasper, J. S.; Watkins, G. D.; Prober, D. E.; Bonner, J. C. *Phys. Rev. B: Solid State* **1976**, *14*, 3036.
(24) Interrante, L. V.; Bray, J. W.; Hard, H. R., Jr.; Kasper, J. S.; Piacente, P. A. *J. Am. Chem. Soc.* **1977**, *99*, 3523.
(25) Bonner, J. C.; Wei, T. S.; Hart, J. R., Jr.; Interrante, L. V.; Jacobs, I. S.; Kasper, J. S.; Watkins, G. D.; Blote, H. W. J. *J. Appl. Phys.* **1978**, *49*, 1321.
(26) Manoharan, P. T.; Noordik, J. H.; de Boer, E.; Keijzers, C. P. *J. Chem. Phys.* **1981**, *74*, 1980.
(27) Ramakrishna, B. L.; Manoharan, P. T. *Inorg. Chem.* **1983**, *22*, 2113.
(28) Persaud, L.; Langford, C. H. *Inorg. Chem.* **1985**, *24*, 3562.
(29) Sano, M.; Adachi, H.; Yamatera, H. *Bull. Chem. Soc. Jpn.* **1981**, *54*, 2636.
(30) Kobayashi, A.; Sasaki, Y. *Bull. Chem. Soc. Jpn.* **1977**, *50*, 2650.

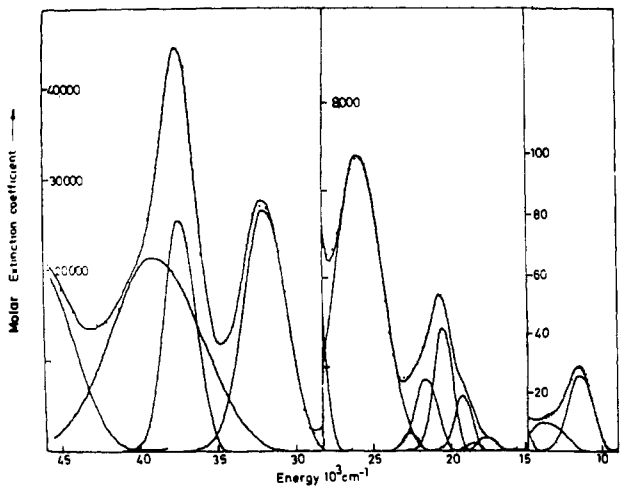

Figure 2. Absorption spectrum of $[(n\text{-}Bu)_4N]_2[Ni(mnt)_2]$ in acetonitrile solution at 298 K as an energy plot and its Gaussian fitting. The dotted line shows the experimental spectrum. Continuous lines show the calculated curves.

is more clearly demonstrated in the Gaussian fitting (Figure 2). The presence of a similar band at 13 880 cm^{-1} has been reported by Schrauzer and Mayweg[14] for $[NiS_4C_4H_4]^{2-}$. This again proves the similarity of the optical spectrum of all metal dithiolenes irrespective of their substituent groups. It is quite true that in some cases the resolutions have been so poor that the presence of some bands with low intensity could not be identified.

The experimental polarized spectra of a single crystal of $[(n\text{-}Bu)_4N]_2[Ni(mnt)_2]$ parallel and perpendicular to the crystallographic c axis in the bc plane are shown in Figure 3a. Since some of the bands appear as if they are shifted on change of polarization, we carried out a deconvolution[31] after conversion into an energy plot. The deconvoluted Energy plots parallel and perpendicular to the crystallographic c axis are shown in Figure 3b. The thinness of the crystal does not permit us to differentiate between the x and y polarizations. Hence, we refer to only $\parallel$ and $\perp$ polarizations with respect to the crystallographic c axis.

The single-crystal spectra (both unpolarized and polarized) at room temperature are made up of three regions centered at 12 000, 20 800, and 26 300 cm^{-1} that show further resolutions. Furthermore, there is a distinct difference in the intensities of bands centered at 20 800 and 26 300 cm^{-1} (crystals vs. solution). While the peak intensity around 20 800 cm^{-1} in solution is smaller than that around 26 300 cm^{-1}, the reverse is true for crystals. This may be due to the presence of a small amount of free ligand in solution, which has an absorption at 26 300 cm^{-1}.

The gross experimental spectrum for the parallel direction shown in Figure 3a is composed of two bands in the infrared region, four reasonably narrow bands and one broad band in the visible region, and one broad band in the ultraviolet region respectively at 11 920, 13 730, 17 990, 19 540, 20 810, and 26 570 cm^{-1}. The perpendicular polarization gives bands at 12 190, 13 960, 18 680, 19 200, 20 560, 22 060, and 27 060 cm^{-1}. A closer look at Figure 3b suggests that the 17 990-cm^{-1} ($\parallel$) band disappears at $\perp$ polarization and is replaced by another band at 18 680 cm^{-1}, which is $\perp$ polarized; similarly the bands at 20 810 and 26 570 cm^{-1} are predominantly present in the parallel polarization and disappear in perpendicular polarization. Instead the two new bands appear at 20 560 and 27 060 cm^{-1}, both of which are definitely perpendicularly polarized. Low-temperature experiments (vide infra) prove this. The other bands appearing in measurements $\parallel$ and $\perp$ to the c axis are perpendicularly polarized.

The room-temperature spectrum measured with use of unpolarized radiation seems to be the combination of the polarized

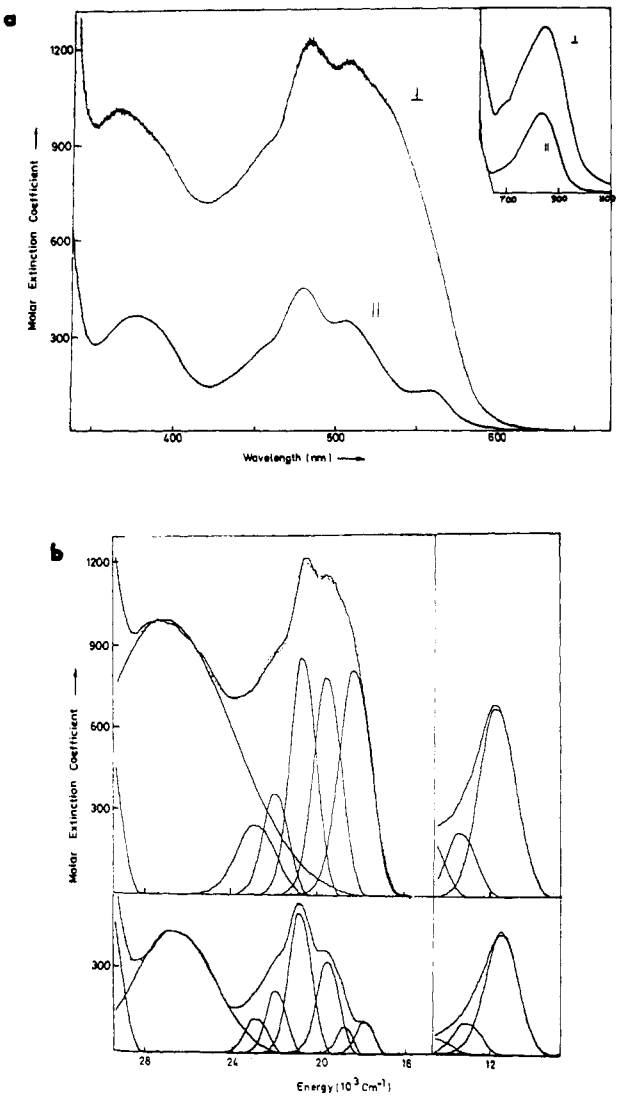

Figure 3. (a) Experimental polarized spectra of single crystal of $[(n\text{-}Bu)_4N]_2[Ni(mnt)_2]$ recorded by keeping the electric vector parallel ($\parallel$) and perpendicular ($\perp$) to the crystallographic c axis in the bc plane with use of a crystal of 0.05-mm thickness. The insert shows the spectrum in the infrared region measured with a crystal of 1.0-mm thickness. (b) The deconvoluted energy plots of (a).

spectra measured $\parallel$ and $\perp$ to the c axis in the bc plane. However, the resolutions are poor in some regions of the spectrum. As the temperature is lowered, there is a continuous increase in the resolution and sharpening of the absorptions in all the regions—infrared, visible, and ultraviolet, accompanied by an overall decrease in the intensity and shifts of some band maxima. This trend continues down to 50 K. Thereafter, as the system is cooled to 18 K, not only does the spectral intensity increase but the spectrum also exhibits a loss of resolution similar to that monitored at high temperature. A careful observation of the band maxima at 50 and 18 K reveals that some of the bands are shifted slightly toward the low-energy region by about 70 cm^{-1}. The reproducibility of this result has been confirmed by measuring the spectra repeatedly while cooling the crystal from 50 to 18 K and also while warming the crystal back to 50 K. The spectral variation in the temperature range 50–298 K is shown in Figure 4a and the same for the temperature range 18–50 K is shown in Figure 4b.

The two low-energy bands in the infrared region (see the deconvoluted spectra in Figure 3b) should be forbidden because of the considerable decrease in the intensity at lower temperatures. The first two bands in the visible region at 17 950 and 19 800 cm^{-1} at room temperature are considerably broad. They not only decrease in intensity as the temperature is lowered to 50 K but also show vibronic progression. For example, the band at 17 950

(31) (a) Barker, B. E.; Fox, M. F. *Chem. Soc. Rev.* **1980**, *9*, 143. (b) Though a deconvolution program was kindly supplied by Dr. Burkhart, G. L. Department of Chemistry, University of Nevada, it was suitably modified to run on a computer with BASIC language facility.

Table I. Electronic Spectra (cm^{-1}) of $[Ni(mnt)_2]^{2-}$

soln in acetonitrile (298 K)[a]	polzd single cryst (298 K)[a]		polarizn	single cryst using unpolzd light		allowed (A)/ forbidden (F)
	∥ (38°)	⊥ (82°)		298 K	50 K	
11 680	11 920	12 190	⊥	12 050	12 200	F
13 750	13 730	13 960	⊥	14 300	14 500	F
					14 660	
					15 240	
					15 820	
					16 390	
					17 500	
18 060	17 990		∥	17 950	18 020	F
					18 420	
18 960		18 680	⊥		18 800	F
					19 230	
19 780	19 540	19 200	⊥	19 800	19 880	F
					20 320	
21 130	20 810		∥	20 920	21 050	A
		20 560	⊥		21 270	A
22 200	22 110[c]	22 060[c]	⊥	21 930	22 270	A
					23 040	
23 170		23 050	⊥	22 990	23 580	A
					24 390	
26 580	26 570		∥	26 810		F
		27 060	⊥		27 320	A
31 300	31 850[b]	31 850[b]		30 770	30 760	A
38 600						A

[a] Band maxima after deconvolution. [b] Not measured due to high absorption. [c] Actually made up of two bands as seen in the low-temperature spectrum.

cm^{-1} in its low-energy tail exhibits at least five peaks due to vibronic progression, the exact energies of which are given in Table I. In addition, though the band at 18 680 cm^{-1} found in the single-crystal spectra in their ⊥ polarization was not even visible in the room-temperature unpolarized spectrum, its presence is revealed as the temperature is lowered, with a maximum around 18 420 cm^{-1} with at least two peaks corresponding to the vibronic progression. Similarly the band at 19 800 cm^{-1} is an extremely broad peak at room temperature but sharpens up and considerably reduces in intensity as the temperature is lowered to 50 K. This broad peak at room temperature seemingly contributes a sizable extent to the height of the higher energy allowed band at 20 560 cm^{-1}. Since the broadening and the intensity of the band at 19 800 cm^{-1} are reduced at lower temperatures, the next higher energy peak is also lower in height. Hence, the first three-band systems in the visible region mentioned above are forbidden due to the symmetry of the molecule. Similarly, the band centered at 26 570 cm^{-1} in ∥ polarization of the single-crystal measurements is also very broad (see Figure 3b). But as the temperature is lowered, the overall intensity of this band decreases, leaving behind only the allowed component centered at 27 060 cm^{-1} in the ⊥ polarization of single-crystal spectra at room temperature. The band at 26 570 cm^{-1} is also responsible for reducing the height of its neighboring bands in the low-energy region as the temperature is lowered. Hence, the broad band system in the region 25 000–28 600 cm^{-1} is actually composed of two bands, one allowed band centered at 27 060 cm^{-1} and one forbidden band centered at 26 570 cm^{-1}. The other bands at 20 810, 21 930, and 22 990 cm^{-1} are all allowed though there seems to be a decrease in their intensities with decrease in temperature. It must be said that this decrease is a manifestation of lowering of the intensities of the two broad bands centered at 19 200 and 26 570 cm^{-1}. The results are given in Table I along with the allowedness and polarization. An attempt at correlating the solution spectrum, the unpolarized single-crystal spectrum at 50 K, and the polarized single-crystal spectra can be made at this stage.

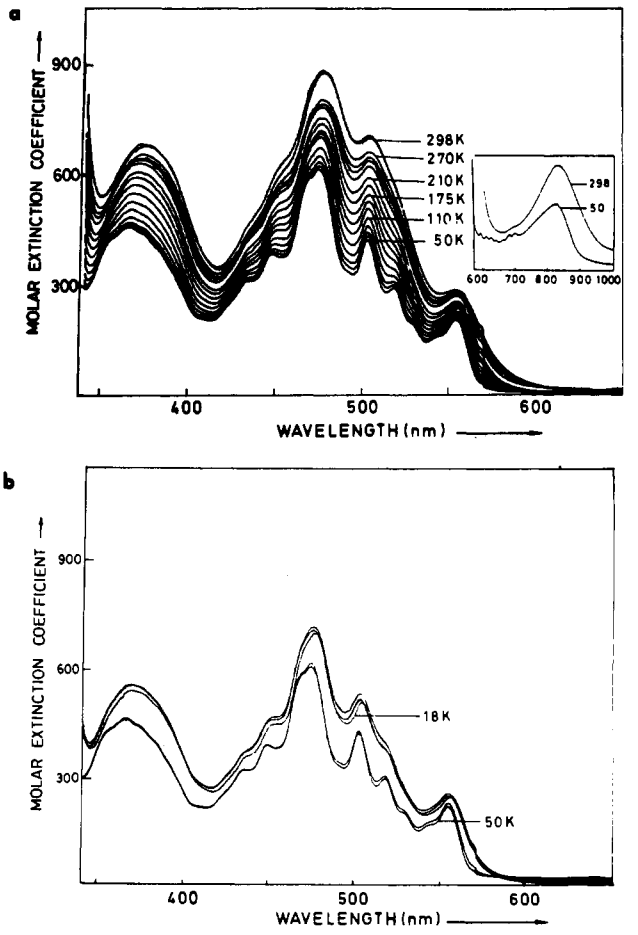

Figure 4. (a) Electronic spectra of a single crystal of $[(n\text{-Bu})_4N]_2[Ni(mnt)_2]$ with unpolarized light in the temperature range 50–298 K. The insert shows the spectra in the infrared region. (b) Spectra of this crystal in the temperature range 18–50 K. The shoulder at 570 nm is due to instrumental error.

Discussion

A. Molecular Orbitals. Before we discuss the assignments for the various electronic transitions obtained from the single crystals, it is necessary to summarize the state of the art available at present on the various molecular orbital calculations. First of all there seem to be two different sets of coordinate systems used by different authors, while our coordinate system given in Figure 1b is similar to that of Gray and co-workers[12] and Schrauzer and Mayweg;[14] Maki et al.,[15] Schmitt and Maki,[16] and Sano et al.[29] used a coordinate system in which the y axis is the bisector of the

Table II. Electronic Spectrum of $[Ni(mnt)_2]^{2-}$ and Assignments of the Transitions

major abs from single cryst (298 K), cm^{-1} (polarizn)	allowed (A)/ forbidden (F)	assignts[a] SBCWG	SM	this work	enabling vib/ nature of charge transfer[c]
12 190 (⊥)	F	$^1A_g \rightarrow {}^1B_{1g}$ ($4a_g \rightarrow 3b_{1g}$)	$^1A_g \rightarrow {}^1B_{1g}$ ($x^2 - y^2 \rightarrow xy$)	$^1A_g \rightarrow {}^1B_{3g}$ ($xz + L \rightarrow xy$)	A_u or B_{1u}
13 960 (⊥)	F	not obsd	$^1A_g \rightarrow {}^1B_{3g}$ ($xz \rightarrow xy$)	$^1A_g \rightarrow {}^1B_{1g}$ ($x^2 - y^2 \rightarrow xy$)	B_{3u} or B_{2u}
17 990 (∥)	F	$^1A_g \rightarrow {}^1B_{2g}$ ($4b_{2g} \rightarrow 3b_{1g}$)	$^1A_g \rightarrow {}^1B_{2u}$, $^1B_{3u}$ ($n_{=s:} \rightarrow M$)	$^1A_g \rightarrow {}^1B_{2g}$ ($yz \rightarrow xy$)	B_{3u}
18 680 (⊥)	F	nob obsd	not obsd	$^1A_g \rightarrow {}^1B_{1g}$ ($z^2 \rightarrow xy$)	B_{3u}, B_{2u}
19 200 (⊥)	F	$^1A_g \rightarrow {}^1A_u$ ($4a_g \rightarrow 3a_u$)	$^1A_g \rightarrow {}^1B_{1g}$ ($n_{=s:} \rightarrow M$)	$^1A_g \rightarrow {}^1B_{3g}$ ($xz \rightarrow xy$)	A_u, B_{1u}
20 560 (⊥)	A	$^1A_g \rightarrow {}^1B_{2u}$ ($4b_{2g} \rightarrow 3a_u$)	$^1A_g \rightarrow {}^1B_{2u}$ ($3b_{2g} \rightarrow 2a_u$)	$^1A_g \rightarrow {}^1B_{2u}$ ($xz \rightarrow a_u$)	$M \rightarrow L_{\pi^*}$
20 810 (∥)	A			$^1A_g \rightarrow {}^1B_{1u}$ ($x^2 - y^2 \rightarrow b_{1u}$)	$M \rightarrow L_{\pi^*}$
21 930 (⊥)	A	not obsd	not obsd	$^1A_g \rightarrow {}^1B_{3u}$ ($yz \rightarrow a_u$)	$M \rightarrow L_{\pi^*}$
22 990 (⊥)	A	not obsd	not obsd	$^1A_g \rightarrow {}^1B_{3u}$ ($b_{3u} \rightarrow xy$)	$L_\pi \rightarrow M$
26 570 (∥)	F	$^1A_g \rightarrow {}^1B_{2u}$ ($2b_{2u}$, $2b_{3u} \rightarrow 3b_{1g}$)	$^1A_g \rightarrow {}^1B_{1g}$ ($n_{=s:} \rightarrow M$)	$^1A_g \rightarrow {}^1B_{1g}$ ($n_{=s:} \rightarrow M$)[b]	B_{3u}, B_{2u}
27 060 (⊥)	A	$^1A_g \rightarrow {}^1B_{2u}$ ($2b_{2u}$, $2b_{3u} \rightarrow 3b_{1g}$)	not obsd	$^1A_g \rightarrow {}^1B_{2u}$ ($b_{2u} \rightarrow xy$)	$L_\pi \rightarrow M$
31 850	A	$^1A_g \rightarrow {}^1B_{2u}$, $^1B_{3u}$ ($3b_{1u} \rightarrow 4b_{3g}$)	not obsd	$^1A_g \rightarrow {}^1B_{2u}$, $^1B_{3u}$	$L_\pi \rightarrow L_{\pi^*}$
38 600	A	$^1A_g \rightarrow {}^1B_{2u}$, $^1B_{3u}$ ($1b_{2u}$, $1b_{3u} \rightarrow 3b_{1g}$)	not obsd	$^1A_g \rightarrow {}^1B_{2u}$, $^1B_{3u}$ (b_{2u}, $b_{3u} \rightarrow xy$)	$L_\sigma \rightarrow M$

[a] In the assignments quoted from ref 12 (SBCWG) and ref 14 (SM) we have retained their original notation. For our assignments please follow Figure 5. [b] Though Schrauzer and Mayweg have not assigned this band in $[Ni(mnt)_2]^{2-}$, they have given this assignment to a corresponding band in $[Ni(mnt)_2]^-$. [c] All the transitions are induced by an electric dipole mechanism.

carbon–carbon double bond of the dithiolene ligand. Hence, we have transformed the results of the last three groups of authors to fit our coordinate system. Second, the ordering of the most important one-electron orbitals obtained by Wolfsberg–Helmholz molecular orbital calculations,[12] simple molecular orbital calculations,[14] discrete variational Xα calculations,[29] and EPR results[11,16] are

(i) WHMO[12]

$$\underset{z^2}{3a_g} < \underset{yz}{3b_{3g}} < \underset{L_\pi}{3b_{1u},2b_{2u},2b_{3u},2b_{1g}} < \underset{xy}{4b_{2g}} < \underset{x^2-y^2}{4a_g} < \underset{xy}{3b_{1g}}$$

(ii) simple MO[14]

$$\underset{xz}{2b_{2g}} < \underset{z^2}{3a_g} < \underset{yz}{2b_{3g}} < \underset{x^2-y^2}{4a_g} < \underset{xz+L}{3b_{2g}} < \underset{xy}{3b_{1g}}$$

(iii) discrete variational Xα method[29]

$$\underset{xz}{4b_{2g}} < \underset{z^2}{19a_g} < \underset{L}{6b_{1u}} < \underset{x^2-y^2}{20a_g} < \underset{yz}{4b_{3g}} < \underset{xz+L}{5b_{2g}} < \underset{xy}{15b_{1g}}$$

(iv) EPR on $[Ni(mnt)_2]^-$[15,16]

$b_{2g}(xz)$ is the highest occupied orbital

$b_{1g}(xz)$ is the lowest unoccupied orbital

In all the above cases the orbital numbers are different due to the differences in the number of basis orbitals used in the calculations. In cases other than the WHMO calculation, the highest occupied molecular orbital has a b_{2g} representation having a substantial ligand contribution to the metal xz orbital while the lowest unoccupied orbital is of a $b_{1g}(xy)$ type species. However, the earlier WHMO calculation predicted $a_g(x^2 - y^2)$ as the highest occupied orbital. Fortunately, the later molecular orbital calculations performed by Gray and his co-workers[33,34] on the paramagnetic square-planar nickel dithiolene anion complexes predict that the half-filled molecular orbital is of $b_{2g}(xy)$ symmetry, rather than the previously obtained a_g, thereby closing a chapter on a serious discrepancy between various workers. In addition, the composition of the highest occupied orbital has also been a matter of great dispute. From the ligand hyperfine and ^{61}Ni hyperfine tensors the half-filled b_{2g} molecular orbital has been found to be roughly 50% delocalized over the ligands,[15,16] while the simple molecular orbital calculations predicted only 18% xz character for the same orbital. This seemingly has been corrected with use of a recent calculation of the ground-state configuration of $[NiS_4C_4H_4]^-$ by means of an extended ω technique by which 51% metal character has been accorded to the half-filled b_{2g} molecular orbital[16] in agreement with the experimental results mentioned above. Combining judicially all these energy level schemes, we have attempted to assign all the observed electronic transitions in conformity with the following scheme containing all the metal orbitals and some ligand orbitals:

$$\underset{xz}{b_{2g}} < \underset{z^2}{a_g} < \underset{yz}{b_{3g}} < \underset{L_\pi}{b_{1u},b_{2u},b_{3u},b_{1g}} < \underset{x^2-y^2}{a_g} < \underset{xz+L}{b_{2g}} <$$

other ligand orbitals L_{π^*}, L_{σ^*}

B. Electronic Spectrum of $[Ni(mnt)_2]^{2-}$. The electronic spectrum of $[Ni(mnt)_2]^{2-}$ can be broadly classified into the d → d type of bands and the M → L and L → M types of bands. The rich optical spectrum of this compound gives 12 bands in the energy region 12 000–32 000 cm^{-1}. Of them, the first five are d → d bands and the remainder are charge-transfer transitions. The final spectral data without vibronic progression, polarizations, allowed and forbidden nature, and assignments are given in Table II.

(i) d → d Type of Bands. First of all, it should be mentioned that the molecule possesses a D_{2h} symmetry and hence the d → d transitions are all parity forbidden. In $[Ni(mnt)_2]^{2-}$, Shupack et al. could identify only two d → d bands and Schrauzer and Mayweg could identify only one. All other transitions have been assigned by them to charge-transfer transitions. Unlike them, we are able to locate all the d → d transitions since we have obtained a more highly resolved spectrum than that of the previous workers. The first five low-energy transitions have been found to be of the d → d type. The lowest energy band at 12 190 cm^{-1} has been assigned to the $^1A_g \rightarrow {}^1B_{3g}$ transition involving the promotion of an electron from the highest occupied $xz + L$ to the lowest unoccupied xy orbital in contrast to the assignments given by the previous workers as $x^2 - y^2 \rightarrow xy$. This is an electric-dipole-allowed transition with vibronic mechanism, the enabling vibration being A_u or B_{1u}. The reason for this assignment will be made clear soon. The shoulder at 13 960 cm^{-1} has not been

(32) For the sake of convenience all the d orbitals are referred to as z^2, $x^2 - y^2$, xz, yz, and xy throughout the text.
(33) Baker-Howkes, M. J. Ph.D. Thesis, Columbia University, 1967.
(34) See footnote 13 in ref 16.

Table III. Orbital and Interelectronic Repulsion Energies of the Ground and Excited States[a] for $[Ni(mnt)_2]^{2-}$ (D_{2h})

spectroscopic state[b]	orbital energy	Slater–Condon energy diff
^1A_g	ground state	
$^1B_{3g}$ $(xz + L \rightarrow xy)$	Δ_1	$-3F_2 - 20F_4$
$^1B_{1g}$ $(x^2 - y^2 \rightarrow xy)$	$\Delta_1 + \Delta_2$	$-35F_4$
$^1B_{2g}$ $(yz \rightarrow xy)$	$\Delta_1 + \Delta_2 + \Delta_3$	$-3F_2 - 20F_4$
$^1B_{1g}$ $(z^2 \rightarrow xy)$	$\Delta_1 + \Delta_2 + \Delta_3 + \Delta_4$	$-4F_2 - 15F_4$
$^1B_{3g}$ $(xz \rightarrow xy)$	$\Delta_1 + \Delta_2 + \Delta_3 + \Delta_4 + \Delta_5$	$-3F_2 - 20F_4$

[a] For d → d transitions only. [b] One-electron excitations leading to the given excited states are shown in parentheses.

observed in this compound by the previous workers. However, a similar band has been revealed in $[NiS_4C_4H_4]^{2-}$ in the work of Schrauzer.[14] Our assignment $^1A_g \rightarrow {}^1B_{1g}$ $(x^2 - y^2 \rightarrow xy)$ is in contrast to $xz \rightarrow xy$ excitation proposed by Schrauzer and Mayweg. Again this is a forbidden transition allowed with a vibronic mechanism with the enabling vibrations B_{3u} and B_{2u} involving a ring deformation or ν(C–S).[35]

The assignment given by Schrauzer and Mayweg to the band at 17 990 cm^{-1} as an allowed transition may be incorrect, because their assignment assumes an allowed charge-transfer excitation while the intensity of this band decreases as the temperature is lowered, indicating its forbidden nature. Similarly, though, the assignment given by Shupack et al. for this band assumes a vibronic mechanism and hence its forbidden nature, which must be perpendicularly polarized while our experiment unequivocally reveals its parallel polarization. We have assigned it to a d → d transition, $^1A_g \rightarrow {}^1B_{2g}$ $(yz \rightarrow xy)$, as an electric dipole excitation with B_{3u} enabling vibration,[35] to account for both its polarization and forbidden nature.

The next band at 18 680 cm^{-1} has not been observed by any of the previous workers since it is not observable in the solution spectra reported by them. This is given the assignment $^1A_g \rightarrow {}^1B_{1g}$ $(z^2 \rightarrow xy)$, with the excited-state enabling vibration[35] B_{2u} or B_{3u}. The presence of vibrational progression with a separation of about 400 cm^{-1} possibly corresponds to a ν(Ni–S) stretching mode (A_g species).

Finally the band at 19 200 cm^{-1} in the series has been assigned as charge-transfer excitation by both earlier groups of workers. This may be incorrect, first because of its forbidden nature and second, even according to the energy level scheme of Schrauzer and Mayweg,[14] ligand to metal charge-transfer transitions should occur at much higher energy. Moreover, the intensities of these bands are comparable to those of the two earlier assigned d → d bands in the visible region. This may be due to $^1A_g \rightarrow {}^1B_{3g}$ $(xz \rightarrow xy)$ excitation. This transition may be observed with an enabling vibration of A_u, B_{1u} species making this perpendicularly polarized as in the case of the band at 12 190 cm^{-1}. However, while the 12 190-cm^{-1} band is an $xz + L \rightarrow xy$ transition, the 19 200-cm^{-1} band is an $xz \rightarrow xy$ transition with a large amount of metal character in the xz orbital as shown in WHMO ($3b_{2g} \rightarrow 3b_{1g}$),[12] simple MO ($2b_{2g} \rightarrow 3b_{1g}$),[14] and DV X$\alpha$ ($4b_{3g} \rightarrow 15b_{1g}$)[29] calculations. The vibronic progression could have merged into the low-energy bands.

We now attempt to substantiate the above assignments as the d → d type, as well as the ordering of the energy levels suggested by us, on the basis of a simple crystal field model for this D_{2h} molecule, as has been done by Gray and Ballhausen[36] and Perumareddy and co-workers[37] for the D_{4h} species. The orbital and interelectronic repulsion energies of the ground and excited states of interest for the above d → d transitions for this D_{2h} complex ion are given in Table III. According to all the earlier molecular orbital calculations[12,14,29] and EPR results[15,16] all the orbitals given in our energy level scheme have large ligand components; for example, from the Xα calculations $4b_{2g}(xz)$, $19a_g(z^2)$, $20a_g(x^2 - y^2)$, $4b_{3g}(yz)$, and $5b_{2g}(xz + L)$ have respectively 65%, 84.9%, 85.4%, 60.5%, and 28.5% metal character and the EPR results[15,16] attribute 50% metal character to $5b_{2g}(xz + L)$ in contrast to the DV Xα method. Because of the extensive delocalization on the ligands, we have assumed a reduction in the electron repulsion energy. Normally for most of the transitions, the Slater–Condon parameter $F_2 = 10F_4$ is given a value of 1000 cm^{-1} for first-row transition-metal ions. Because of the extensive delocalization on the ligands, we have taken $F_2 = 10F_4 = 750$ cm^{-1} for this complex in close analogy to the value of 700 cm^{-1} for $[M(CN)_4]^{2-}$ complexes.[36] By comparing the experimental energies the various d → d transitions assigned above with the energy expressions given in Table III, we have calculated the values of the orbital energies as $\Delta_1 = 15\,940$ cm^{-1}, $\Delta_2 = 645$ cm^{-1}, $\Delta_3 = 5155$ cm^{-1}, $\Delta_4 = 1064$ cm^{-1}, and $\Delta_5 = 145$ cm^{-1}.

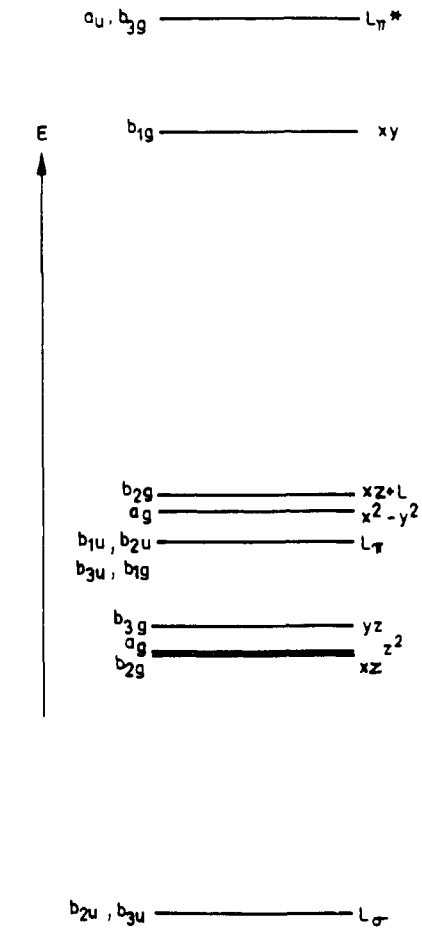

Figure 5. Energy level diagram proposed by us for $[(n\text{-Bu})_4N]_2[Ni(mnt)_2]$ (only important levels included).

Thus the ordering of the energy levels is consistent with the energy level scheme proposed by us above. In addition, at least our d-level scheme is quite comparable to the one proposed by Shupack et al.[12] except for the interchange of $x^2 - y^2$ and $xz + L$ levels, which in their scheme correspond to $4a_g$ and $4b_{2g}$. It is, however, comforting to see that our proposed ordering of energy levels now conforms with the later work by Gray and co-workers.[33,34] Thus, our corrected energy level scheme is given in Figure 5.

(ii) Charge-Transfer Transitions. The remaining transitions from 20 560 cm^{-1} onward pertain to charge-transfer transitions. Of them, the transitions at 20 560, 20 810, and 21 930 cm^{-1} are metal to ligand (π^*) charge-transfer transitions. The assignments given are based on the energy level diagram given in Figure 5. The corresponding transitions have also been noted in earlier work except that their complete assignments have been hampered by the loss of resolution, which we monitored at low temperature. Similarly, there are two ligand to metal transitions in square-planar halide complexes. However, the reduction in symmetry to D_{2h}

(35) Schlapfer, C. W.; Nakamoto, K. *Inorg. Chem.* **1975**, *14*, 1338.
(36) Gray, H. B.; Ballhausen, C. J. *J. Am. Chem. Soc.* **1963**, *85*, 260.
(37) Perumareddy, J. R.; Liehr, A. D.; Adamson, A. W. *J. Am. Chem. Soc.* **1963**, *85*, 249.

may have created one more, particularly the π type. Hence, the band at 22 990 cm^{-1} has been assigned to $L_\pi \rightarrow M$.

The band at 26 570 cm^{-1} is the only forbidden charge-transfer transition from ligand to metal that we could observe in $[Ni(mnt)_2]^{2-}$. The difficulty in the assignment of this band by the earlier workers could have come from the fact that this band in combination with an allowed band at 27 060 cm^{-1} forms a very broad absorption with a full width at half-maximum of nearly 7000 cm^{-1}, making it difficult to even guess the presence of two components. However, our polarized optical work in combination with the low-temperature work clearly brings out the forbidden nature of the former band and the allowedness of the latter. Particularly the temperature-dependence study indicates the combination of the 26 570- and 27 060-cm^{-1} bands at room temperature, which progressively shows the evolution of the 27 060-cm^{-1} band accompanied by the disappearance of the 26 570-cm^{-1} band (Figure 4a). This must have caused Shupack et al.[12] to assign the broad band as their transition $L_\pi \rightarrow M$ ($2b_{3u}$, $2b_{2u} \rightarrow 3b_{1g}$). Though this assignment is wrong for the parallel-polarized band at 26 570 cm^{-1}, it holds good for the perpendicularly polarized one at 27 060 cm^{-1}. Similarly, Schrauzer and Mayweg assigned a band similar to 26 570 cm^{-1} in $[Ni(mnt)_2]^-$ to $^1A_g \rightarrow {}^1B_{1g}$ ($n_{=S} \rightarrow M$). We concur with their assignment for the forbidden band at 26 570 cm^{-1}. Moreover, some of the charge-transfer transitions in the square-planar halide complexes are known to be of $L \rightarrow M$ type.[36] Typically they exhibit two bands separated approximately by 10 000 cm^{-1} with higher energy bands being considerably more intense. Our assignment of this band at 27 060 cm^{-1} is in complete accord with that of Shupack et al.[12] as an $L \rightarrow M$ charge-transfer transition, while the other transition of the same type does occur at high energy, 38 600 cm^{-1}. The band at 31 850 cm^{-1} is an $L \rightarrow L^*$ transition since it corresponds to the first absorption in bis((methylthio)maleonitrile) at about 30 000 cm^{-1}.[12]

C. Temperature Dependence from 18 to 50 K. It is quite surprising that the intensities of all the transitions increase below 50 K. This could be tentatively interpreted as due to a lowering of the symmetry of the complex ion, making all the transitions allowed. The following experimental facts lend support to this tentative conclusion: (i) no new transitions have been observed at temperatures below 50 K; (ii) the bands observed above 50 K do not disappear when the system is cooled below 50 K; (iii) some of the bands moved to lower energies at temperatures below 50 K. The increase in intensity accompanied by a decrease in transition energies can hence be explained by a departure from the planarity of $Ni(mnt)_2^{2-}$ anion. In other words, the symmetry of the anion responsible for the entire electronic spectrum could have changed from D_{2h} to D_2 by creating a dihedral angle between the two ligand planes attached to the same metal atom. Such exceptional nonplanarity has been found in some of the dithiolene complexes.[38-42]

Recently we have observed two phase transitions,[43] one at 50 K and another around 20 K, when we studied the ESR of $Cu(mnt)_2^{2-}$ doped in $[(n\text{-}Bu)_4N]_2[Ni(mnt)_2]$. The carefully measured ESR spectra further reveal a slight change in the "g" and "A" tensors of the $Cu(mnt)_2^{2-}$ ion, giving evidence to distortions from planarity. Detailed work is under way.

Conclusions

A combination of the polarized spectra of single crystals of $[(n\text{-}Bu)_4N]_2[Ni(mnt)_2]$ with a low-temperature isotropic study has thrown considerable light on the rich electronic spectra of the complex ion. Though we have interpreted the electronic spectra on the basis of a scheme proposed by us, the rich optical spectral data necessitates a new molecular orbital calculation in order to confirm the nature of electronic excitations suggested in this work. Furthermore, experiments below 50 K suggest the deviation of this dithiolene complex from planarity.

Acknowledgment. We gratefully acknowledge the Department of Science and Technology, Government of India, for financial support to carry out this work.

Registry No. $[(n\text{-}Bu)_4N][Ni(mnt)_2]$, 18958-57-1.

(38) Snaathorst, D.; Doesburg, H. M.; Perenboom, J. A. A. J.; Keijzers, C. P. *Inorg. Chem.* **1981**, *20*, 2526.
(39) Venkatalakshmi, N.; Babu Varghese; Williams, R. F. X.; Manoharan, P. T., unpublished observations.
(40) Hamilton, W. C.; Bernal, I. *Inorg. Chem.* **1967**, *6*, 2003.
(41) Enemark, J. H.; Lipscomb, W. N. *Inorg. Chem.* **1965**, *4*, 1729.
(42) Baker-Hawkes, M. J.; Dosi, Z.; Eisenberg, R.; Gray, H. B. *J. Am. Chem. Soc.* **1968**, *90*, 4253.
(43) Chandramouli, G. V. R.; Manoharan, P. T., unpublished results.

Contribution from the Department of Chemistry, Colorado State University, Fort Collins, Colorado 80523

Theoretical Characterization of Nitrogen Fixation: Effect of Ligand on the Initial Dinitrogen Activation

A. K. Rappé

Received May 9, 1986

Correlated ab initio theoretical calculations at the valence double-ζ level are used to study the effect of metal (molybdenum and tungsten) and ligand (fluorine, chlorine, and bromine) on the relative stability of activated (azine) vs. unactivated forms of bridging dinitrogen. We find a pronounced (26 kcal/mol) effect of halogen substitution for the molybdenum complexes $[MoX_4N]_2$. For the tungsten analogues we find only a minor variation (9 kcal/mol) with halogen substitution. For all three halogen complexes the activated form of N_2 (azine) is substantially more stable than the unactivated classical structure for tungsten. For molybdenum, even with halogen variation the unactivated form is more stable than the activated form.

Introduction

The activation and reduction of dinitrogen under mild conditions is a process of interest in heterogeneous catalysis,[1] homogeneous reactivity and structural studies,[2-10] and theoretical studies.[11-17]

$$N_2(g) + 3H_2(g) \rightarrow 2NH_3(g) \quad (1)$$

The ΔG_{300K} for this reaction is -7.9 kcal/mol.[18] Industrially, this

(1) (a) Ertl, G. *Catal. Rev.—Sci. Eng.* **1980**, *21*, 201-223. (b) Boudart, M. *Catal. Rev.—Sci. Eng.* **1981**, *23*, 1-15. (c) Nieken, A. *Catal. Rev.—Sci. Eng.* 17-51. (d) Ozaki, A. *Acc. Chem. Res.* **1981**, *14*, 16-21. (e) *Riegel's Handbook of Industrial Chemistry*; Kent, J. A., Ed.; Van Nostrand Reinhold: New York, 1983; pp 143-221.

(2) (a) Chatt, J.; Dilworth, J. R.; Richards, R. L. *Chem. Rev.* **1978**, *78*, 589-625. (b) Henderson, R. A.; Leigh, G. J.; Picket, C. J. *Adv. Inorg. Chem. Radiochem.* **1983**, *27*, 197-292.

0020-1669/86/1325-4686$01.50/0